



**HAL**  
open science

## **Mass Diffusion and Thermal Diffusivity of the Decane-pentane Mixture Under High Pressure as a Ground-based Study for SCCO Project**

I. Lizarraga, C. Giraudet, Fabrizio Croccolo, M.M. Bou-Ali, Henri Bataller

► **To cite this version:**

I. Lizarraga, C. Giraudet, Fabrizio Croccolo, M.M. Bou-Ali, Henri Bataller. Mass Diffusion and Thermal Diffusivity of the Decane-pentane Mixture Under High Pressure as a Ground-based Study for SCCO Project. *Microgravity Science and Technology*, 2016, 28 (5), pp.545-552. <10.1007/s12217-016-9506-9>. <hal-01815883>

**HAL Id: hal-01815883**

**<https://hal.science/hal-01815883v1>**

Submitted on 6 Feb 2020

**HAL** is a multi-disciplinary open access archive for the deposit and dissemination of scientific research documents, whether they are published or not. The documents may come from teaching and research institutions in France or abroad, or from public or private research centers.

L'archive ouverte pluridisciplinaire **HAL**, est destinée au dépôt et à la diffusion de documents scientifiques de niveau recherche, publiés ou non, émanant des établissements d'enseignement et de recherche français ou étrangers, des laboratoires publics ou privés.



HAL Authorization

1        **Mass diffusion and thermal diffusivity of the decane-pentane**  
2        **mixture under high pressure as a ground-based study for SCCO**  
3        **project**

4        Ion Lizarraga<sup>1</sup>, Cédric Giraudet<sup>2</sup>, Fabrizio Croccolo<sup>2</sup>, M. Mounir Bou-Ali<sup>1</sup>, and Henri  
5        Bataller<sup>2</sup>

6        <sup>1</sup> *MGEP Mondragon Goi Eskola Politeknikoa, Mechanical and Industrial Manufacturing*  
7        *Department, Loramendi 4 Apdo. 23, 20500 Mondragon, Spain*

8        <sup>2</sup> *Laboratoire des Fluides Complexes et leurs Réservoirs, UMR-5150, Université de Pau et*  
9        *des Pays de l'Adour, 1 Allée du Parc Montaury, Anglet, FR.*

10  
11        **Abstract**

12        Thermodiffusion experiments on iso-massic binary mixture of decane and pentane in the  
13        liquid phase have been performed between 25°C and 50°C and for pressures from 1MPa until  
14        20MPa. By dynamic analysis of the light scattered by concentration non-equilibrium  
15        fluctuations in the binary mixture we obtained the mass diffusion coefficients of the mixture  
16        at each temperature and pressure. For the first time we were able to apply similar analysis to  
17        thermal fluctuations thus getting a simultaneous measurement of the thermal diffusivity  
18        coefficient. While mass diffusion coefficients decrease linearly with the pressure, thermal  
19        diffusivity coefficients increase linearly. In principle the proposed method can be used also  
20        for measuring the Soret coefficients at the same time. However, for the present mixture the  
21        intensity of the optical signal is limited by the optical contrast factor. This affects our  
22        capability of providing a reliable estimate of the Soret coefficient by means of dynamic  
23        Shadowgraph. Therefore the mass diffusion coefficients measurements would need to be  
24        combined with independent measurements of the thermodiffusion coefficients, e.g.  
25        thermogravitational column, to provide Soret coefficients. The obtained values constitute the

26 on-ground reference measurements for one of the mixture studied in the frame of the project  
27 SCCO-SJ10, which aims to measure the Soret coefficients of multicomponents mixtures  
28 under reservoir conditions. Microgravity experiments will be performed on the Chinese  
29 satellite SJ10 launched in April 2016.

30

31 **Keywords:** mass diffusion, thermal diffusivity, decane-pentane mixture, non-equilibrium

32 fluctuations, high pressure, SCCO, SJ10

## 33 1. Introduction

34 The precise modelling of the distribution of chemical species in oil and gas reservoirs remains  
35 a topical issue for the oil industry, especially now that the reserves of fossil fuels are getting  
36 more difficult to extract. It is known that not only gravitational segregation, but also  
37 thermodiffusion due to geothermal gradients, are two physical phenomena determining the  
38 vertical distribution of species in hydrocarbon reservoirs on Earth (Lira-Galeana et al. 1994,  
39 Høier et al. 2001, Ghorayeb et al. 2003, Montel et al. 2007). Thermodiffusion, or Soret effect,  
40 is a phenomenon that couples heat and mass fluxes (de Groot and Mazur 1984) and can also  
41 lead to convective unstable conditions in particular cases (Galliero et al. 2009). The  
42 contribution of thermodiffusion is difficult to quantify, mainly due to a lack of experimental  
43 data as well as accurate modeling for multicomponent mixtures. Although noticeable  
44 progresses have been made during the last twenty years, (Assael et al., 2014 and references  
45 therein) especially on ternary mixtures both theoretically (Firoozabadi et al., 2000; Kempers,  
46 2001; Galliero et al., 2003) and experimentally (Leahy-Dios et al., 2005; Larrañaga et al.,  
47 2015; Gebhardt et al., 2015), more work is necessary. Micro-gravity experiments, to avoid  
48 gravity-induced convection, are one possible way to provide further data on thermodiffusion  
49 in multicomponent mixtures (Georis et al., 1998; Van Vaerenbergh et al., 2009; Touzet et al.,  
50 2011; Bou-Ali et al., 2015). The Soret Coefficients in Crude Oil (SCCO) project aims at  
51 producing values of Soret coefficients of mixture of petroleum interest and in reservoirs  
52 conditions. In a first phase carried out in 2007 microgravity experiments were performed on  
53 board the Russian satellite FOTON-M3. One binary, two ternaries and one quaternary  
54 mixtures were studied (Van Vaerenbergh et al., 2009; Srinivasan et al., 2009; Touzet et al.,  
55 2011). The measurements were compared with molecular dynamics simulations and with  
56 theoretical calculations based on the Thermodynamics of Irreversible Processes. However, the  
57 conclusions were incomplete because of difficulties encountered during post flight analysis at

58 the laboratories (Touzet et al., 2011). Now, on the occasion of the China Sea well  
59 explorations, a second phase of the SCCO space experiment has been scheduled. The  
60 thermodiffusion behaviour of the binary mixture decane-pentane, the ternary mixture decane-  
61 heptane-pentane and the quaternary mixture decane-heptane-pentane-methane, at two  
62 pressures and at 50°C, will be studied on-board the Shijian-10 (SJ-10) Chinese satellite during  
63 2016 (Galliero et al., 2015). To assure the success of this new mission, both validating ground  
64 measurements and numerical simulations have been planned. In this paper we present results  
65 on the iso-massic binary mixture decane-pentane based on the measurement of non-  
66 equilibrium (NE) fluctuations.

67 In general, from the analysis of the dynamics of concentration NE fluctuations by light-  
68 scattering it is possible to measure the fluid transport properties coefficients, including the  
69 mass diffusion and Soret coefficients, as demonstrated for binary mixtures (Croccolo et al.,  
70 2012, 2014). The technique has been adapted to high pressure (Giraudet et al., 2014). In this  
71 work we extend the technique to the analysis of thermal fluctuations thus including the  
72 possibility of measuring the thermal diffusivity coefficient of the mixture. Conversely, due to  
73 the limited amplitude of the optical signal obtained for this system, we were not able here to  
74 measure the Soret coefficient.

75 The remainder of the paper is organized as follows: Section 2 reports the methodology, in  
76 Section 3 we provide results and discussion, and in Section 4 conclusions are drawn.

77

## 78 **2. Methodology**

79

### 80 *Theoretical background*

81 In a homogeneous multicomponent mixture a temperature gradient induces heat transfer as  
82 well as segregation of the components along the temperature gradient by means of the Soret

83 effect (de Groot and Mazur, 1984). The segregation induces then Fickian diffusion and the  
 84 combination of the two phenomena results in a steady concentration gradient which is  
 85 convection-free only in microgravity conditions or in particular cases on ground. A  
 86 thermodiffusion experiment on ground is typically performed by applying a stabilizing  
 87 thermal gradient to a multicomponent fluid mixture, thus obtaining a superposition of the  
 88 mentioned phenomena. Even if there is no total mass flux in the steady state, thermal and  
 89 concentration NE fluctuations are always present. NE fluctuations are strictly related to the  
 90 transport properties of the fluid. That is why from NE fluctuations analysis one can determine  
 91 in principle all transport coefficients, like viscosity, thermal diffusivity and solutal diffusion  
 92 and thermodiffusion coefficients. A detailed description of the theory of NE fluctuations can  
 93 be found in the book by Ortiz de Zárate and Sengers (Ortiz de Zárate and Sengers, 2006).  
 94 Here we briefly recall the essential equations that will be used in the following.

95 In a binary mixture, the temporal correlation function of NE concentration fluctuations  
 96 induced by the Soret effect is expected to be a single exponential decay for all wave vectors,  
 97 with time constants  $\tau_s(q)$  varying as a function of the wave vector  $q$ . For wave vectors much  
 98 larger than a characteristic value  $q_s^*$ , the decay time is the solutal diffusive one:

99

$$100 \quad \tau_s(q) = 1/(Dq^2), \quad (\text{Eq. 1})$$

101

102 where  $D$  is the mass diffusion coefficient. NE thermal fluctuations are faster and overlap to  
 103 the solutal ones. For wave vectors larger than a thermal characteristic wave vector  $q_T^*$ , the  
 104 decay time is the thermal diffusive one:

105

$$106 \quad \tau_T(q) = 1/(\kappa q^2), \quad (\text{Eq. 2})$$

107

108 where  $\kappa$  is the thermal diffusivity coefficient.

109

### 110 *Experimental set-up*

111 Our thermodiffusion cell (Fig.1 of Giraudet et al., 2014) is specifically designed for applying  
112 a vertical temperature gradient with excellent thermal homogeneity and stability to a  
113 horizontal slab of a multicomponent fluid under high pressure while providing vertical optical  
114 access to a central area of the cell. The cell core consists of a stainless steel annulus of  
115 internal/external diameter 30/75mm with high pressure inlet and outlet at its opposite sides.  
116 This part accommodates Teflon®-coated Viton® O-rings for sealing, and square sapphire  
117 plates kept at a distance  $L = 5\text{mm}$  by the annulus itself, thus defining the sample thickness. In  
118 order to minimize the contact between the liquid sample and the conductive metal a Teflon  
119 annulus (internal/external diameter 19.8/30mm) with two thin holes (diameter 1mm) for  
120 inlet/outlet of the fluid has been inserted in the inner part of the stainless annulus zone.

121 The external sides of the sapphire windows are in thermal contact with two aluminium plates  
122 with a central circular aperture ( $d=13\text{mm}$ ), where two thermistors (Wavelength Electronics,  
123 TCS651) are installed to monitor the sapphire temperatures. External to the aluminium plates,  
124 two Peltier elements (Kryotherm, TB-109-1.4-1.5 CH) with central circular aperture  
125 ( $d=13\text{mm}$ ) provide/remove the heat necessary to maintain the set-point temperature as driven  
126 by two temperature controllers (Wavelength Electronics, LFI-3751) maintaining the  
127 temperature of the internal side of each Peltier device with a stability better than 1mK RMS  
128 over 1 day. Finally, external to the Peltier elements, two aluminium plates are flushed with  
129 water coming from a thermostatic bath (Huber, ministat 125) to remove the excess heat of the  
130 Peltiers.

131 Experiments have been performed with the iso-massic binary mixture of decane (Sigma-  
132 Aldrich,  $\geq 99\%$ ) and pentane (Sigma-Aldrich,  $\geq 99\%$ ). Components were used without further

133 purification. The mixture is prepared in a bottle by weighting on a balance (Sartorius,  
134 TE313S, resolution  $10^{-2}$ g/200g) first the decane and then the pentane. The bottle is carefully  
135 closed by cover with Teflon sealing. Error in mass fraction is estimated less than  $\pm 0.0001$ .

136 The filling system consists of: a rotary vacuum pump able to evacuate most of the air from the  
137 cell before filling operations down to a residual pressure of about 10Pa; a fluid vessel at  
138 atmospheric pressure; a manual volumetric pump and a number of valves to facilitate the  
139 procedure. Briefly, after a low vacuum is made inside the cell, the mixture to be studied is  
140 transferred to the cell by acting on the volumetric pump. Visual check allows avoiding  
141 bubbles during the injection procedure. After that, the cell is abundantly fluxed with the fluid  
142 mixture. At the end of the procedure a valve is closed and the volumetric pump is operated to  
143 modify the liquid pressure within the cell. A manometer (Keller, PAA-33X, pressure range:  
144  $0.1 \div 100$ MPa, precision  $\pm 0.04$ MPa) is connected between the volumetric pump and the cell to  
145 measure the pressure of the fluid mixture. A second identical manometer is connected to the  
146 outlet of the cell. The manometer signals are transferred using an acquisition card (National  
147 Instruments, NI 9215) interfaced to a computer.

148 We perform our experiments by imposing a difference of temperature  $\Delta T$  on the horizontally  
149 positioned thin cell, previously filled with the homogenous fluid mixture.

150 In order to investigate NE fluctuations, it is common to use a scattering in the near field  
151 technique as the Shadowgraph (Wu et al. 1995), for which the physical optics treatment was  
152 given by Trainoff and Cannell (2002) and Croccolo and Brogioli (2011). The shadowgraph  
153 optical setup involves a low coherence light source (Super Lumen, SLD-MS-261-MP2-SM,  $\lambda$   
154  $= 675 \pm 13$ nm) that illuminates the bottom of the cell through a single-mode fiber. The  
155 diverging beam exiting from the fiber end is collimated by an achromatic doublet lens ( $f =$   
156  $150$ mm,  $\phi = 50.8$ mm) and then passes through a linear film polarizer. In combination with a  
157 second linear polarizer after the cell the latter allows us to adapt the average light intensity.

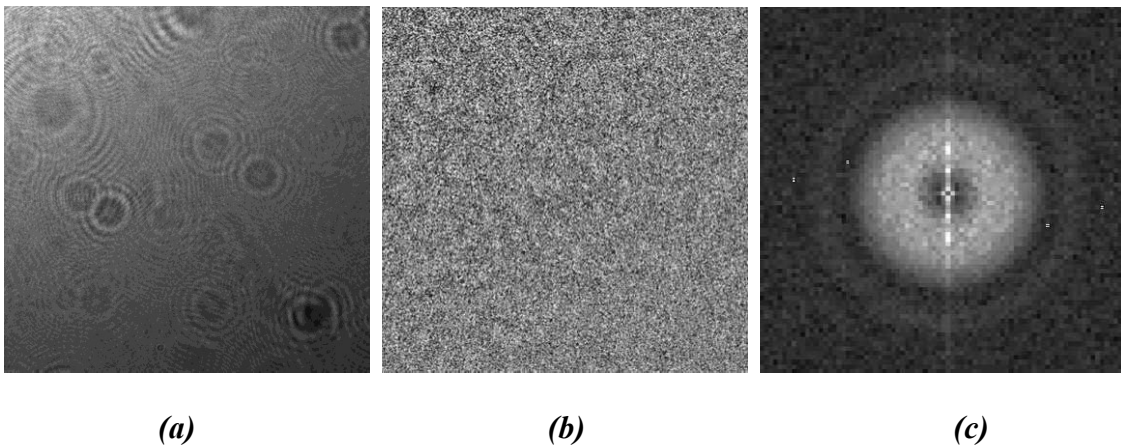
158 The detection plane is located at about  $z = 95\text{mm}$  from the sample plane. As a sensor, we use  
159 a charge coupled device (AVT, PIKE-F421B) with  $2048 \times 2048$  square pixels each of size  $7.4$   
160  $\times 7.4\mu\text{m}^2$  and a dynamic range of 14-bit. Images were cropped within a  $768 \times 768\text{pix}^2$  in order  
161 to reach the maximum acquisition frame rate of the camera of about 30Hz.

162

### 163 *Dynamic near-field imaging*

164 Images acquired by means of a near-field scattering setup consist of an intensity map  $I(\vec{x}, t)$   
165 generated by the interference on the CCD plane between the portion of the incident beam that  
166 has passed undisturbed through the sample and the beams scattered by refractive index  
167 fluctuations occurring within the sample (Trainoff and Cannell, 2002; Croccolo and Brogioli,  
168 2011). Statistical analysis involving fast Fourier transforms provides accurate measurements  
169 of the intensity  $I_s(\vec{q}, t)$  of light scattered at each wave vector  $\vec{q}$  grabbed by the optical setup  
170 and for all the times  $t$  of the acquisition sequence. Different setups show different responses to  
171 the acquired signal as a function of the wave number  $q$ , which is described by the so-called  
172 transfer function  $T(q)$ .

173



176 **Figure 1:** Results of a near field scattering experiment (shadowgraph layout) on the iso-  
177 massic binary of decane and pentane stressed by a thermal gradient ( $T_{mean} = 50^\circ\text{C}$ ,  $P = 20$

178  $MPa, \Delta T = 30^\circ C$ ). (a)  $768 \times 768 \text{ pix}^2$  near field image of the sample,  $I(\vec{x}, t)$  (b) image  
179 difference,  $\Delta I(\vec{x}, \Delta t) = I(\vec{x}, t + \Delta t) - I(\vec{x}, t)$ , having a correlation time of  $\Delta t = 0.35 \text{ s}$  and (c)  
180 2D Fast Fourier Transform squared  $|I(\vec{q}, t + \Delta t) - I(\vec{q}, t)|^2$  of (b).

181

182 Details of the quantitative dynamic analysis can be found elsewhere (Croccolo et al., 2006a;  
183 Croccolo et al., 2006b; Croccolo et al., 2007; Cerchiari et al., 2012). Here we just recall that  
184 the quantity directly obtained from the experiments is the so-called structure function  
185  $C_m(q, \Delta t) = \langle |\Delta I_m(q, \Delta t)|^2 \rangle$ , that is obtained by averaging (over all available times  $t$  in each  
186 image dataset and over the wave vector  $\vec{q}$  azimuthal angle) the individual spatial Fourier  
187 transforms of the shadowgraph image differences, like the one shown in the example of Fig.  
188 1. This experimental structure function is theoretically related to the temporal correlation  
189 function of NE composition fluctuations, also called intermediate scattering function (*ISF*),  
190 by:

191

$$192 \quad C_m(q, \Delta t) = 2\{S(q)T(q)[1 - ISF(q, \Delta t)] + B(q)\}, \quad (\text{Eq.3})$$

193

194 with  $ISF(q, 0) = 1$ . In Eq.3,  $S(q)$  is the static power spectrum of the sample,  $T(q)$  is the optical  
195 transfer function and  $B(q)$  the background noise of the measurement. It is implicitly assumed  
196 in Eq.3 that the linear response of the CCD detector and any other electronic or  
197 electromagnetic proportionality parameters are aggregated inside  $T(q)$  and/or  $B(q)$ .

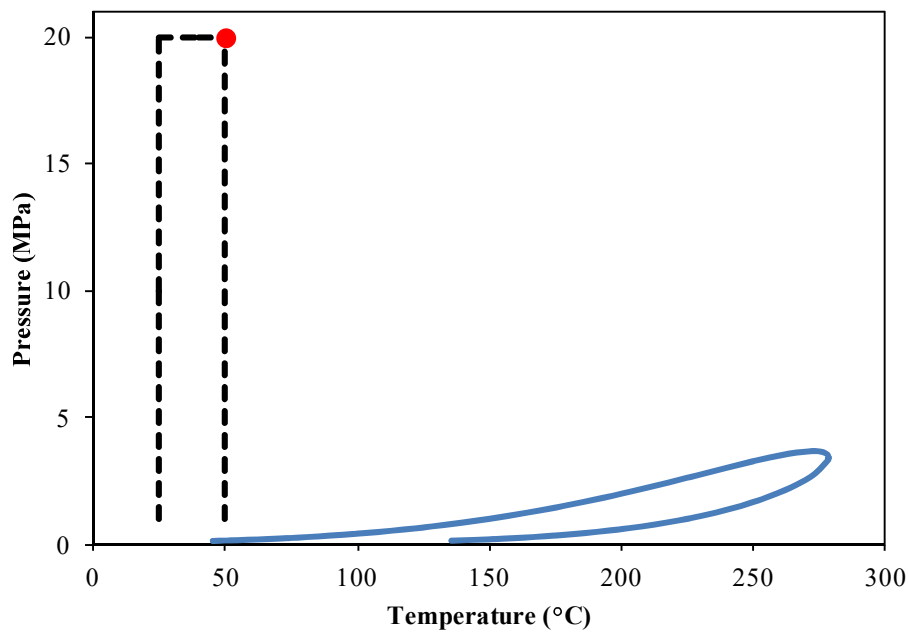
198

### 199 **3. Results and Discussion**

200

#### 201 ***Thermodynamic conditions***

202 To determine the thermodynamic conditions of the study, we have calculated, with TOTAL  
 203 S.A. company BEST software, the biphasic envelop and critical coordinates of the iso-massic  
 204 binary mixture of decane and pentane. For a given pressure  $P$  and a given temperature  $T$ , the  
 205 software calculates the possible molar volumes  $v$  from the PPR78 equation of state (Peng and  
 206 Robinson, 1976). In Fig.2 we report the calculated biphasic envelop.  
 207



208  
 209 **Figure 2:** Phase diagram of the isomassic binary mixture decane-pentane: the continuous  
 210 line represents the biphasic envelop. The dashed lines represent the values of pressure and  
 211 temperature investigated for the reported thermodiffusion experiments. The red point  
 212 indicates the thermodynamic conditions of the thermodiffusion experiment shown in Fig. 1, 3  
 213 and 4 ( $T_{mean} = 50^{\circ}\text{C}$ ,  $P = 20 \text{ MPa}$ ).

214  
 215 In Fig.2 the dashed line represents the values of pressure and temperature investigated for  
 216 the present thermodiffusion experiments, the temperature of  $50^{\circ}\text{C}$  being imposed by the  
 217 microgravity experimental conditions of the SCCO project, and the temperature of  $25^{\circ}\text{C}$   
 218 being selected as the experimental data references for mass diffusion coefficients only exist at

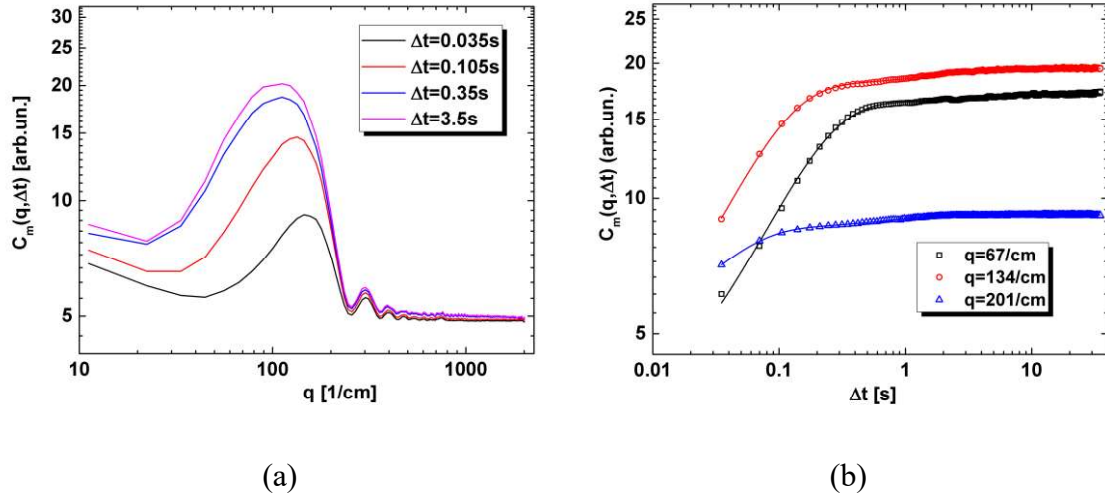
219 this temperature. Initially, a temperature difference of  $20^{\circ}\text{C}$  was applied to the system. To  
220 increase the optical signal, which remains low as revealed by Fig.1b-c, we applied a  
221 temperature difference of  $30^{\circ}\text{C}$ . In all the investigated conditions the mixture was in its liquid  
222 state, even at low pressure and for temperature differences of  $\Delta T = 20$  and  $30^{\circ}\text{C}$ . The red  
223 point in Fig.2 indicates the thermodynamic conditions of the thermodiffusion experiment  
224 shown in Fig.1, 3 and 4 ( $T_{\text{mean}} = 50^{\circ}\text{C}$ ,  $P = 20$  MPa).

225

### 226 *Structure function*

227 At each investigated temperature  $T$  and pressure  $P$ , 10 different image acquisition runs have  
228 been performed with a delay time  $dt_{\text{min}} = 35\text{ms}$  between two consecutive images. Each set,  
229 containing 2000 images, has then been processed on a dedicated PC by means of a custom-  
230 made CUDA/C++ software (Cerchiari et al., 2012), in order to perform a fast parallel  
231 processing of the images to obtain the structure functions  $C_m(q, \Delta t)$ , for all the wave numbers  
232 and for all the correlation times accessible within the image datasets. In each experiment the  
233 temperature gradient is applied via two distinct temperature controllers, so that a linear  
234 temperature gradient sets up in some tens of seconds. The image acquisition is started about  
235 five hours later, to be sure that the concentration gradient due to the Soret effect is fully  
236 developed within the cell.

237 In Fig.3 we present the mean structure function  $C_m(q, \Delta t)$  of the 10 runs a) as a function of the  
238 wave number for different correlation times and b) as a function of the correlation time for  
239 different wave numbers, for mean temperature  $T_{\text{mean}} = 50^{\circ}\text{C}$ , pressure  $P = 20\text{MPa}$  and a  
240 difference of temperature  $\Delta T = 30^{\circ}\text{C}$ . The oscillatory behavior shown in Fig.3a is due to the  
241 optical transfer function  $T(q)$  (see Eq.3). It is typical of shadowgraph experiments and it  
242 corresponds to the ring pattern shown in Fig. 1c.



244

245

246 **Figure 3:** Experimental structure function  $C_m(q, \Delta t)$  (a) as a function of the wave vector  $q$  for  
 247 different correlation times  $\Delta t$  and (b) as a function of the correlation time  $\Delta t$  for different  
 248 wave vectors  $q$  ( $T_{\text{mean}} = 50^\circ\text{C}$ ,  $P = 20\text{MPa}$ ,  $\Delta T = 30^\circ\text{C}$ ).

249

250 Fig.3a shows that for wave numbers  $q > 400\text{cm}^{-1}$ , the signal is completely lost in the  
 251 background noise. For intermediate wave numbers, Fig.3b shows that the time dependence of  
 252 the structure function cannot be totally assumed mono-exponential, as it is visible for wave  
 253 numbers  $q = 134\text{cm}^{-1}$  and  $201\text{cm}^{-1}$ . To account for the solutal relaxation mode plus the  
 254 thermal relaxation mode, we therefore decided to perform a quantitative analysis of the  
 255 experimental structure functions by modeling the *ISF* as a double exponential decay, namely:

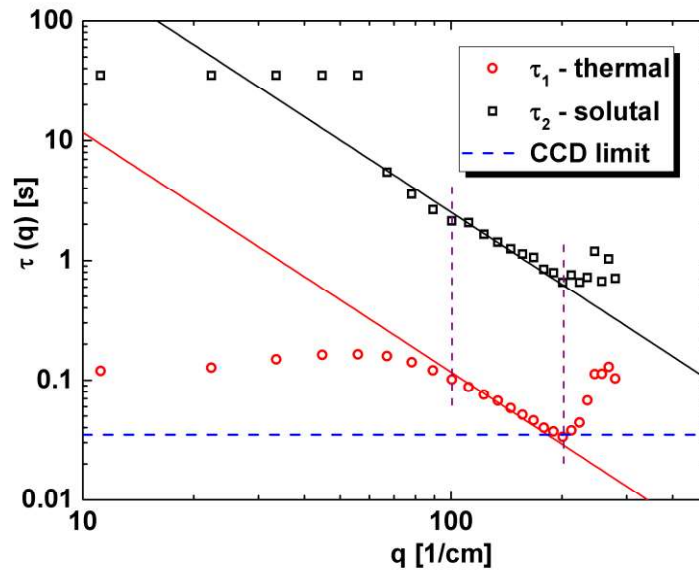
256

$$257 \quad ISF(q, \Delta t) = a \exp\left(-\frac{\Delta t}{\tau_1(q)}\right) + (1-a) \exp\left(-\frac{\Delta t}{\tau_2(q)}\right), \quad (\text{Eq. 4})$$

258

259 where  $\tau_1$  and  $\tau_2$  are two relaxation times. Hence, we performed fittings of the experimental  
 260  $C_m(q, \Delta t)$  as a function of  $\Delta t$  (see Fig.3b) by substituting Eq.4 into Eq.3 and adopting as fitting

261 parameters: the product  $S(q)T(q)$ , the background  $B(q)$ , the relative amplitude  $a$ , and the two  
 262 decay times,  $\tau_1$  and  $\tau_2$ . For the fitting procedure we used a Levenberg-Marquardt Non-Linear  
 263 Least Square fitting algorithm.  
 264



265  
 266 **Figure 4:** Experimental decay times of NE fluctuations as obtained by fitting through Eqs.3  
 267 and 4, as a function of the wave number  $q$ .  $\circ$ : fast mode,  $\square$ : slow mode ( $T_{mean} = 50^\circ\text{C}$ ,  $P =$   
 268  $20\text{MPa}$ ,  $\Delta T = 30^\circ\text{C}$ ). The black solid line represents the theoretical relaxation times  $1/Dq^2$  of  
 269 Eq.1 and the red solid line represents the theoretical relaxation times  $1/\kappa q^2$  of Eq.2.

270  
 271 In Fig.4 we show the two decay times obtained from modeling the *ISF* by Eq.4, as a function  
 272 of the wave number. The horizontal dashed blue line corresponds to  $dt_{\min} = 35\text{ms}$ , which is  
 273 the physical limit of our experimental recording equipment.

274 Intuitively, we assumed that the fastest mode was associated with a thermal mode and the  
 275 slowest to a solutal mode.

276 In the range of wave numbers  $100\text{ cm}^{-1} \leq q \leq 200\text{ cm}^{-1}$  (vertical dotted lines are plotted in Fig.4  
 277 to guide the reader) the slowest mode was fitted with Eq.1 using  $D$  as free parameter and the

278 fastest was fitted with Eq.2 using  $\kappa$  as free parameter. The results of the adjustments are  
 279 reported by continuous lines in Fig.4. For example, referring to the conditions of Fig.4 ( $P =$   
 280  $20\text{MPa}$ ,  $T_{\text{mean}} = 50^\circ\text{C}$ ) the two values obtained by fitting are  $D = (38\pm 4)\times 10^{-6}\text{cm}^2/\text{s}$  and  $\kappa =$   
 281  $(870\pm 40)\times 10^{-6}\text{cm}^2/\text{s}$ . Uncertainties are the average of the deviations respect to the mean value  
 282 of the 10 measurements.

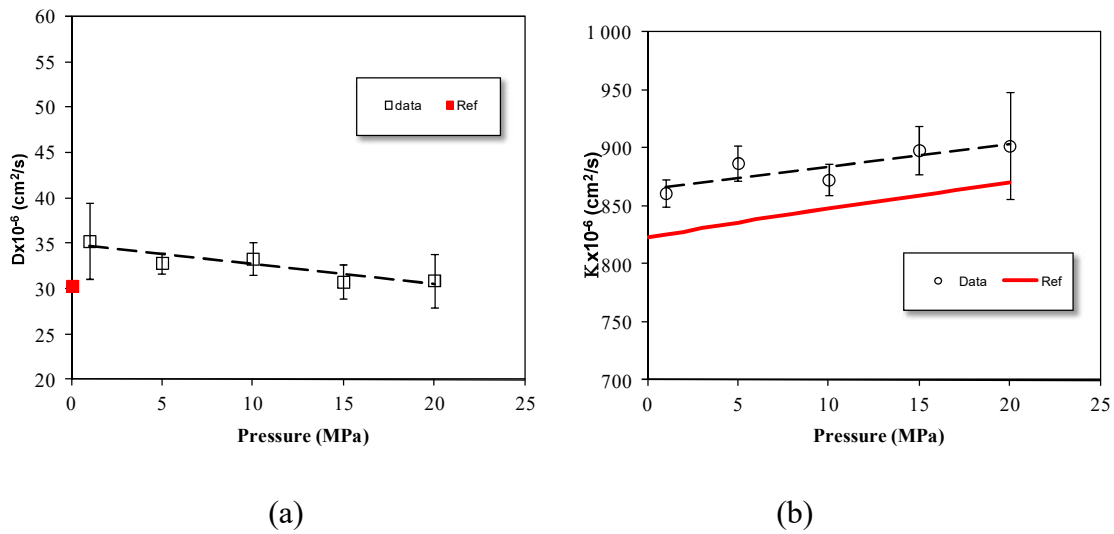
283

284 **Mass diffusion and thermal diffusivity coefficients**

285

286 In Fig.5 we report the values of mass diffusion and thermal diffusivity coefficients as a  
 287 function of the pressure obtained for the iso-massic binary mixture of decane and pentane, at  
 288  $T_{\text{mean}} = 25^\circ\text{C}$  and for a temperature difference  $\Delta T = 20^\circ\text{C}$ .

289



290

291

292 **Figure 5:** Mass diffusion  $D$  and thermal diffusivity  $\kappa$  coefficients as a function of the pressure  
 293 at  $T_{\text{mean}} = 25^\circ\text{C}$  and for a temperature difference of  $\Delta T = 20^\circ\text{C}$ .

294

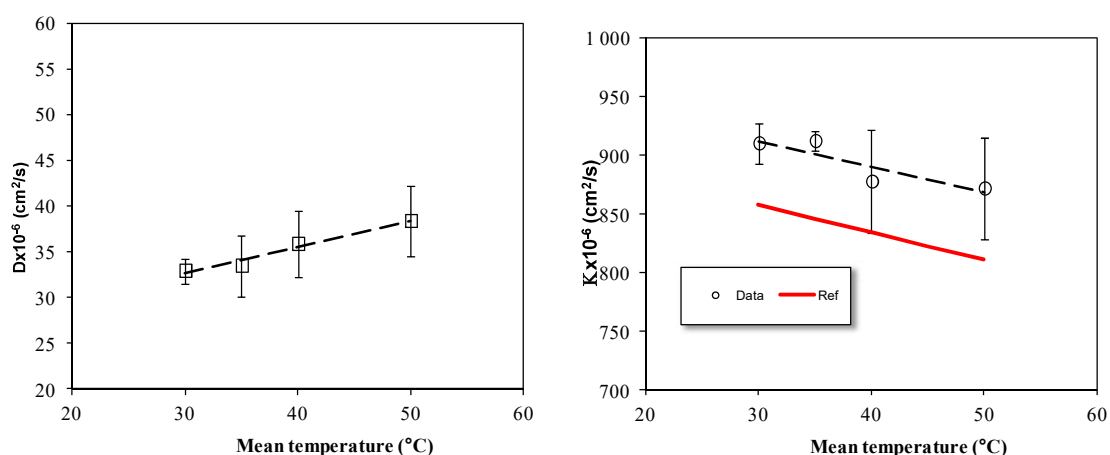
295 We found only one reference value of the mass diffusion coefficients at atmospheric pressure  
 296 (Alonso De Mezquia et al., 2012) that we reported in Fig.5a as a red point. The thermal

297 diffusivity coefficients were compared with values found in NIST data base (NIST website)  
 298 and reported by a red continuous line in Fig.5b. Our values slightly overestimate reference  
 299 values. However, over the entire pressure range studied, the relative deviation of the thermal  
 300 diffusivity coefficients values does not exceed 5%. These results validate our hypothesis for  
 301 the interpretation of the modes of the measured intermediate scattering function, namely that  
 302 the fastest mode is the thermal relaxation mode of NE fluctuations and the slowest a mass  
 303 relaxation mode.

304 In Fig.5a we can notice a slight linear decrease in the mass diffusion coefficient with pressure  
 305 that is consistent with an increase of the viscosity with pressure (mass diffusion coefficient  
 306 being proportional to the inverse of the viscosity), as it has been shown in Alonso De Mezquia  
 307 et al., 2012. Also in Fig.5b we can see a linear increase in the thermal diffusivity coefficients  
 308 with pressure that is consistent with an increase of the density with pressure.

309 In Figure 6 we report the values of mass diffusion and thermal diffusivity coefficients as a  
 310 function of the mean temperature obtained for the iso-massic binary mixture of decane and  
 311 pentane, at  $P = 20\text{MPa}$  and for a temperature difference  $\Delta T = 30^\circ\text{C}$ .

312



313

314

(a)

(b)

315 **Figure 6:** Mass diffusion  $D$  and thermal diffusivity  $\kappa$  coefficients as a function of the mean  
 316 temperature at  $P= 20\text{MPa}$  and for a temperature difference of  $\Delta T = 30^\circ\text{C}$ .

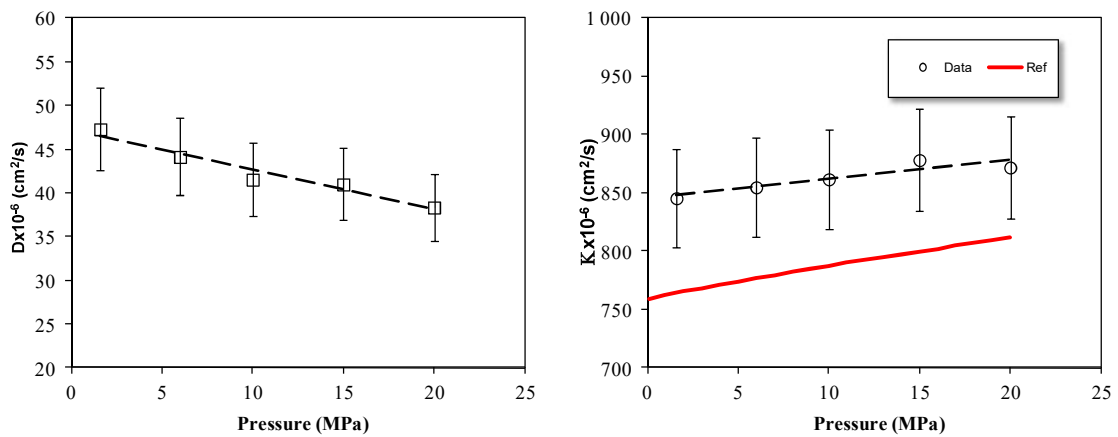
317

318 In Fig.6a we can see that the mass diffusion coefficient increases with the mean temperature,  
 319 which is consistent with a decrease of the viscosity of the system with the mean temperature.

320 In Fig.6b we can see that the thermal diffusivity coefficient decreases with the mean  
 321 temperature. Again an overestimate of the reference values is detected.

322 In Fig.7 we report the values of mass diffusion and thermal diffusivity coefficients as a  
 323 function of the pressure obtained for the iso-massic binary mixture of decane and pentane, at  
 324  $T_{\text{mean}} = 50^\circ\text{C}$  and for a temperature difference  $\Delta T = 30^\circ\text{C}$ . The same trends as for Fig.5 are  
 325 observed.

326



327

328 **Figure 7:** Mass diffusion  $D$  and thermal diffusivity  $\kappa$  coefficients as a function of the pressure  
 329 at  $T_{\text{mean}} = 50^\circ\text{C}$  and for a temperature difference of  $\Delta T = 30^\circ\text{C}$ .

330

#### 331 4. Conclusions

332

333 Thermodiffusion experiments on iso-massic binary mixture of decane and pentane, in the  
334 liquid phase, have been performed between 25°C and 50°C and for pressures from 1MPa until  
335 20MPa. By means of dynamic analysis of the light scattered by concentration NE fluctuations  
336 of the binary mixture we obtained the values of the mass diffusion coefficient  $D$  at each  
337 temperature and pressure. The shadowgraph set-up and its acquisition chain enabled us to  
338 achieve a minimum delay time between two successive images of 35ms. We were thus able to  
339 investigate for the first time temperature NE fluctuations, which let us model the ISF as the  
340 sum of two decreasing exponentials. This procedure allowed obtaining simultaneously the  
341 values of the thermal diffusivity coefficient  $\kappa$ . Mass diffusion coefficients  $D$  decrease with the  
342 pressure while thermal diffusivity coefficients  $\kappa$  increase with the pressure. For the  
343 investigated mixture, due to a limited intensity of the optical signal, it was not possible to  
344 obtain a reliable measurement of the Soret coefficients  $S_T$ . Therefore the obtained values of  
345 the mass diffusion coefficients  $D$  must be combined with thermodiffusion coefficients  $D_T$   
346 measurements obtained by an independent experiment, such as thermogravitational column.  
347 The resulting values at 50°C can be directly compared to measurements made in microgravity  
348 in the frame of the SCCO-SJ10 project.

349

350

### 351 **Acknowledgements**

352 This work has been supported by the European Space Agency through the SCCO project.  
353 Support from the French space agency CNES is also acknowledged. We thank TOTAL S.A.  
354 for allowing the use of the BEST software and Research Groups (No. IT1009-16) and  
355 TERDISOMEZ (No. FIS2014-58950-C2-1-P) of MINECO.

356

### 357 **References**

- 358 - Alonso de Mesquia, D., Bou-Ali, M.M., Larrañaga, M., Madariaga, J.A., Santamaria,  
359 C.: Determination of molecular diffusion coefficient in n-alkane binary mixtures:  
360 Empirical correlations. *J. Phys. Chem. B* 116, 2814-2819 (2012).
- 361 - Assael, M.J., Goodwin, A.R.H., Vesovic, V., Wakeham, W.A.: *Experimental*  
362 *Thermodynamics Volume IX: Advances in Transport Properties of Fluids*, Royal  
363 *Society of Chemistry, London, (2014).*
- 364 - Bou-Ali, M.M., Ahadi, A., Alonso de Mezquia, D., Galand, Q., Gebhardt, M., Khlybov,  
365 O., Köhler, W., Larrañaga, M., Legros, J.C., Lyubimova, T., Mialdun, A., Ryzhkov, I.,  
366 Saghir, M.Z., Shevtsova, V., Van Vaerenbergh, S.: Benchmark values for the Soret,  
367 thermodiffusion and molecular diffusion coefficients of the ternary mixture  
368 tetralin+isobutylbenzene+n-dodecane with 0.8-0.1-0.1 mass fraction. *Eur. Phys. J. E*  
369 38, 30 (2015).
- 370 - Cerchiari, G., Croccolo, F., Cardinaux, F., Scheffold, F.: Quasi-real-time analysis of  
371 dynamic near field scattering data using a graphics processing unit. *Rev. Sci. Instrum.*  
372 83, 106101 (2012).
- 373 - Croccolo, F., Brogioli, D., Vailati, A., Giglio, M., Cannell, D.S.: Use of the dynamic  
374 Schlieren to study fluctuations during free diffusion. *App. Opt.* 45, 2166-2173  
375 (2006a).
- 376 - Croccolo, F., Brogioli, D., Vailati, A., Giglio, M., Cannell, D.S.: Effect of gravity on the  
377 dynamics of non equilibrium fluctuations in a free diffusion experiment. *Ann. N. Y.*  
378 *Acad. Sci.* 1077, 365 (2006b).
- 379 - Croccolo, F., Brogioli, D., Vailati, A., Giglio, M., Cannell, D.S.: Non-diffusive decay of  
380 gradient driven fluctuations in a free-diffusion process. *Phys. Rev. E.* 76, 41112  
381 (2007).

- 382 - Croccolo, F., Brogioli, D.: Quantitative Fourier analysis of schlieren masks: the  
383 transition from shadowgraph to schlieren. *App. Opt.* 50, 3419-3427 (2011).
- 384 - Croccolo, F., Bataller, H., Scheffold, F.: A light scattering study of non equilibrium  
385 fluctuations in liquid mixtures to measure the Soret and mass diffusion coefficient. *J.*  
386 *Chem. Phys.* 137, 234202 (2012).
- 387 - Croccolo, F., Bataller, H., Scheffold, F.: Static versus dynamic analysis of the influence  
388 of gravity on concentration non equilibrium fluctuations. *Eur. Phys. J. E* 37, 105  
389 (2014).
- 390 - de Groot, S.R., Mazur, P.: *Nonequilibrium Thermodynamics*. Dover, New York (1984).
- 391 - Firoozabadi, A., Ghorayeb, K., Shukla, K.: Theoretical model of thermal diffusion  
392 factors in multicomponent mixtures, *AIChE Journal* 46, 892-900, 2000.
- 393 - Galliero, G., Duguay, B., Caltagirone, J.P., Montel, F.: On thermal diffusion in binary  
394 and ternary mixtures by non-equilibrium molecular dynamics, *Phil. Mag.* 83, 2097-  
395 2108 (2003).
- 396 - Galliero, G., Montel, F.: Understanding compositional grading in petroleum reservoirs  
397 thanks to molecular simulations. *Society of Petroleum Engineers Paper.* 121902,  
398 Amsterdam, 2009
- 399 - Galliero, G., Bataller, H., Croccolo, F., Vermorel, R., Artola, P.-A., Rousseau, B.,  
400 Vesovic, V., Bou-Ali, M., Ortiz de Zárate, J.M., Xu, S., Zhang, K., Montel, F.: Impact  
401 of Thermodiffusion on the initial distribution of Species in hydrocarbon reservoirs.  
402 *Microgravity Sci. Technol.* DOI 10.1007/s12217-015-9465-6.
- 403 - Gebhardt M. and Köhler W.: Soret, thermodiffusion, and mean diffusion coefficients of  
404 the ternary mixture ndodecane+ isobutylbenzene+1,2,3,4 tetrahydronaphthalene. *J.*  
405 *Chem. Phys.* 143, 164511 (2015).

- 406 - Georis, P., Montel, F., Van Vaerenbergh, S., Decoly, Y., Legros, J.C.: Proceedings of  
407 the European Petroleum Conference, 1, pp. 57-62 (1998).
- 408 - Ghorayeb, K., Firoozabadi, A., Anraku, T.: Interpretation on the unusual fluid  
409 distribution in the Yufutsu gas-condensate field. SPE J. 8, 114-123 (2003).
- 410 - Giraudet, C., Bataller, H., Croccolo, F.: High-pressure mass transport properties  
411 measured by dynamic near-field scattering of non-equilibrium fluctuations. Eur. Phys.  
412 J. E 37, 107 (2014).
- 413 - Høier, L., Whitson, C.H.: Compositional grading-theory and Practice. SPE Reserv.  
414 Evaluation Eng. 4, 525-532 (2001).
- 415 - Kempers L.J.T.M.: A comprehensive thermodynamic theory of the Soret effect in a  
416 multicomponent gas, liquid, or solid, J. Chem. Phys. 115, 6330-6341 (2001).
- 417 - Larrañaga M., Bou-Ali M., Lizarraga I., Madariaga J.A., Santamaría S.: Soret  
418 Coefficients of the Ternary Mixture 1,2,3,4-Tetrahydronaphthalene + Isobutylbenzene  
419 + N-Dodecane, J. Chem. Phys. 143, 024202 (2015).
- 420 - Leahy-Dios, A., Bou-Ali, M.M., Platten, J.K., Firoozabadi, A.: Measurements of  
421 molecular and thermal diffusion coefficients in ternary mixtures, J. Chem. Phys. 122,  
422 234502 (2005).
- 423 - Lira-Galeana, C., Firoozabadi, A., Prausnitz, J.M.: Computation of compositional  
424 grading in hydrocarbon reservoirs. Application of continuous thermodynamics. Fluid  
425 Phase Equilib. 102, 143-158 (1994).
- 426 - Montel, F., Bickert, J., Lagisquet, A., Galliero, G.: Initial state of petroleum reservoirs:  
427 A comprehensive approach. J. Pet. Sci. Eng. 58, 391-402 (2007).
- 428 - NIST website: <http://webbook.nist.gov/chemistry/>
- 429 - Ortiz de Zárate J.M., Sengers, J.V.: Hydrodynamic Fluctuations in Fluids and Fluid  
430 Mixtures, Elsevier, Amsterdam, (2006).

- 431 - Peng, D.Y., Robinson, D.B.: A new two-constant equation of state. *Ind. Eng. Chem.*  
432 *Fundam.* 15, 59-64 (1976).
- 433 - Srinivasan, S., Saghir, M.Z.: Measurements on thermodiffusion in ternary hydrocarbon  
434 mixtures at high pressure. *J. Chem. Phys.* 131, 124508 (2009).
- 435 - Trainoff, S.P., Cannell, D.S.: Physical optics treatment of the shadowgraph. *Phys. of*  
436 *Fluids* 14, 1340-1363 (2002).
- 437 - Touzet, M., Galliero, G., Lazzeri, V., Saghir, M.Z., Montel, F., Legros, J.C.:  
438 Thermodiffusion: from microgravity experiments to the initial state of petroleum  
439 reservoirs, *Comptes Rendus - Mécanique* 339, 318-323 (2011).
- 440 - VanVaerenbergh, S., Srinivasan S., Saghir, M.Z.: Thermodiffusion in multicomponent  
441 hydrocarbon mixtures: Experimental investigations and computational analysis. *J.*  
442 *Chem. Phys.* 131, 114505 (2009).
- 443 - Wu, M., Ahlers, G., Cannell, D.S.: Thermally induced fluctuations below the onset of  
444 the Rayleigh-Bénard convection. *Phys. Rev. Lett.* 75, 17432-1746 (1995).
- 445